

Thermodynamic properties of LiCu_2O_2 multiferroic compound

Yan Qi and An Du*

College of Sciences, Northeastern University, Shenyang 110819, China

Abstract

A spin model of quasi-one dimensional LiCu_2O_2 compound with ground state of ellipsoidal helical structure in which the helical axis is along the diagonal of CuO_4 squares has been adopted. By taking into account the interchain coupling and exchange anisotropy, the exotic magnetic properties and ferroelectricity induced by spiral spin order have been studied by performing Monte Carlo simulation. The simulation results qualitatively reproduce the main characters of ferroelectric and magnetic behaviors of LiCu_2O_2 compound and confirm the low-temperature incommensurate spiral ordering. Furthermore, by performing the calculations of spin structure factor, we systematically investigate the effects of different exchange coupling on the lower-temperature magnetic transition, and find that the spiral spin order depends not only on the ratio of nearest and next-nearest neighbor inchain spin coupling but also strongly on the exchange anisotropy.

* Author to whom correspondence should be addressed. Electronic mail: duanneu@163.com. Tel.: 086-024-83678326.

I. INTRODUCTION

The multiferroics, in which magnetism and ferroelectricity coexist in the same material, have attracted many researchers since 1960s due to their fundamental physics and potential technological applications [1, 2]. In recent years, the magnetism-driven ferroelectricity discovered in frustrated magnets renews the interest in this field. A simple prototype of frustrated magnets is a spin chain with the nearest-neighbor (NN) ferromagnetic (FM) coupling and the next-nearest-neighbor (NNN) antiferromagnetic (AF) coupling. Such competing interactions can lead to frustration and an incommensurate spiral order in magnetic materials [3]. Actually, a class of low-dimensional cuprate oxides such as LiCuVO_4 , Li_2CuO_2 , $\text{Li}_2\text{ZrCuO}_4$ etc. were reported to have such spiral magnetic orders [4-9]. And it is believed that the research on the ferroelectricity of magnetic origin in these low-dimensional compounds will be helpful in understanding the multiferroic nature [10, 11].

LiCu_2O_2 is a typical representative of multiferroic cuprates with a quantum spin $S=1/2$ [12, 13]. It has an orthorhombic crystal structure with a $Pmna$ space group and unit cell parameters $a=5.73 \text{ \AA}$, $b=2.86 \text{ \AA}$, $c=12.42 \text{ \AA}$. The crystal structure is twinned at the microscopic level in the ab plane as a result of the unit cell parameter a very close to $2b$ [14]. It has an equal number of Cu^{2+} and Cu^{1+} ions in distinct nonequivalent crystallographic positions. The magnetic Cu^{2+} ions are located at the center of edge-sharing CuO_4 plaquettes and form a zigzag like spin-chain structure along the b axis [15-17]. The experimental data reveals that the system undergoes two successive magnetic transitions at $T_{N1}\sim 25\text{K}$ and $T_{N2}\sim 23\text{K}$ [18, 19]. Below T_{N2} , the ferroelectricity emerges with the spiral magnetic order. At $T_{N2}<T<T_{N1}$, the intermediate state is found to be a sinusoidal spin state.

Although many experiments and theoretical studies on LiCu_2O_2 have been performed [20-24], the nature of the ground state and the origin of the ferroelectricity remain under debate. Masuda et al. carried out an unpolarized neutron diffraction study and firstly proposed the incommensurate helimagnetic order in ab plane [15]. However, based on this ab -spiral picture, the fact that the polarization emerges along the c axis can not be interpreted by the commonly accepted microscopic mechanisms: the inverse Dzyaloshinskii-Moriya interaction or spin-current model. Later, Park et al. suggested another spin picture that the transverse spiral spin component was in the bc -plane [7], which is partially confirmed by Seki et al.,

but the quantitative calculation on the intensity of polarized neutron reflections shows a prominent discrepancy [19]. Recently, based on their own NMR and neutron diffraction data, Sato et al. proposed a new noncollinear modulated magnetic structure. They pointed out that the magnetic structure of LiCu_2O_2 in the low-temperature phase ($T < T_{N2}$) is an ellipsoidal structure with the helical axis tilted by about 45° from the a - or b - axis within the ab plane [10, 11]. This 45° -tilt spin model receives strong evidence support from the very recent experiments performed by Li et al [14]. However, as far as we know, the corresponding theoretical investigations based on this new model are still absent.

In this paper, with the consideration of interchain coupling and exchange anisotropy, a spin model of LiCu_2O_2 with ground state of the ellipsoidal helical structure has been employed. Monte Carlo simulation is carried out to investigate the fascinating magnetoelectric coupling behaviors in this multiferroic compound. Our simulation qualitatively reproduces the experimental results of the complicated electric and magnetic behaviors observed in LiCu_2O_2 , confirming the spiral spin order at ground state. In addition, the influences of the different exchange interactions and easy-plane anisotropies on the lower-temperature magnetic phase pattern have also been explored. The spin structure factors are calculated to analyze the variations of the underlying microscopic magnetic and ferroelectric structures. We believe that the present work will be helpful in understanding the ferroelectricity in frustrated magnets and shed some additional light on this interesting physical subject.

II. MODEL AND SIMULATION

LiCu_2O_2 is a complex spin-driven ferroelectricity multiferroic compound. Its magnetism stems from the two linear Cu^{2+} chains, which propagate along the b axis and form a zigzag ladderlike structure. These ladders are isolated from each other by both Li ions and the layers of non-magnetic Cu^{1+} ions. The sketch map of the magnetic structure is demonstrated in Fig. 1, which can be regarded as an equivalent quasi-one dimensional Bravais lattice of spins [15, 16]. The Hamiltonian of this system can be written in the following general form

$$H = \sum_{i,j} J_{ij}(S_i^a S_j^a + S_i^b S_j^b + \Delta S_i^c S_j^c) - D \sum_i (\mathbf{S}_i \cdot \mathbf{e}_i)^2 - \mathbf{h} \cdot \sum_i \mathbf{S}_i - \mathbf{h}_e \cdot \sum_i \mathbf{P}_i, \quad (1)$$

where (S_i^a, S_i^b, S_i^c) are the classical spin components with unit vectors. $\Delta \leq 1$ is the exchange anisotropy, usually presenting in low-dimensional system with multiple magnetic transitions [25]. Theoretically, an XXZ-type anisotropy ($\Delta \lesssim 1$) is expected to stabilize a vector chiral order [22]. And recent experiment also shows that substantial exchange anisotropies exist in the edge-sharing spin-chain compounds [26]. In order to yield results that much close to those of experiments, the value of $\Delta=0.7$ is adopted here. J_{ij} represents exchange coupling between spins on different site. As a result of the Cu-O-Cu bond angles near 94° , the NN FM inchain coupling J_2 and NNN AF inchain coupling J_4 are expected from the Kanamori-Goodenough rule [9]. The estimated ratio $|J_4/J_2|$ has been experimentally verified to vary from 0.50 to 0.65 [15, 24]. However, upon the values of J_1 and J_\perp , it is still a subject of discussion at present. Based on inelastic neutron scattering experiments and spin wave theory, Masuda et al.[27] suggest a strong AF "rung" interaction J_1 and a weak inter-chain coupling J_\perp , while Drechsler et al. obtain a contrary conclusion through the analysis of electronic structure and cluster calculations [9]. Irrespective of this dispute, we adopt the suggestion of Masuda et al. here. Our simulation also qualitatively demonstrates a good agreement with the results of experiments under the condition of a strong J_1 coupling. Thus, unless particularly stated, the default values of J_1 , J_2 , J_4 and J_\perp are set as 3.4, -6.0, 3.0 and 0.9 respectively in this paper, which is slightly different from those determined from the spin-wave spectra in the proportion of exchange constants.

Considering the 45° -tilt spin model proposed by Sato et al. (Fig. 2), a plane anisotropy has been added in the Hamiltonian. D represents the magnitude of the magnetic anisotropy. \mathbf{e}_i is a unit vector and in the direction of [110], representing the direction of magnetic anisotropy. Due to the large negative value of anisotropy, $D=-5$, a spiral magnetic order forming in the [110] plane can be expected. And this kind of anisotropy will lead to a strong spin coupling along c axis, and therefore plays an essential role for the emergency of spontaneous polarization [28]. According to the observation of the low temperature magnetic structure, Sato et al.[10, 11] have confirmed that the relation $\mathbf{P} \propto \mathbf{Q} \times \mathbf{e}_3$ holds in LiCu_2O_2 compound, where \mathbf{P} , \mathbf{Q} and \mathbf{e}_3 are the ferroelectric polarization, the modulation vector and the helical axis of the ordered spins. This indicates that the theories derived by phenomenological[29] and microscopic models [30–32] are also applied for polarization of LiCu_2O_2 . Thus, according to the spin current model, or equivalently, the inverse Dzyaloshinskii-Moriya interaction, \mathbf{P}_i induced by the neighboring canting spins (\mathbf{S}_i and \mathbf{S}_j)

is expressed as follows:

$$\mathbf{P}_i = -A\mathbf{e}_{ij} \times (\mathbf{S}_i \times \mathbf{S}_j), \quad (2)$$

where \mathbf{e}_{ij} denotes the vector connecting the two sites of \mathbf{S}_i and \mathbf{S}_j , namely in the direction of magnetic modulation vector along the b axis. A is a proportional constant determined by the spin-exchange and the spin-orbit interactions as well as the possible spin-lattice coupling term. It is assumed to be unity here. Judging from this relation, the spontaneous polarization along the c axis observed in the experiment can be expected. Consequently, the third and fourth items in Hamiltonian Eq. (1) correspond to magnetic and electric energies, where \mathbf{h} is the external magnetic field including an extra factor $g\mu_B$ and \mathbf{h}_e is the external electric field.

According to the statistical definitions and thermal fluctuations, the general expressions for those quantities concerned in this paper can be written in the following form:

$$m_\alpha = \frac{1}{N} \sum_i S_i^\alpha, \quad (3)$$

$$P_\alpha = \frac{1}{N} \sum_i P_i^\alpha, \quad (4)$$

$$\chi_m^\alpha = \frac{1}{NT} (\langle M_\alpha^2 \rangle - \langle M_\alpha \rangle^2), \quad (5)$$

$$\chi_e^\alpha = \frac{1}{NT} (\langle P_\alpha^2 \rangle - \langle P_\alpha \rangle^2), \quad (6)$$

$$C_m = \frac{1}{NT^2} (\langle H^2 \rangle - \langle H \rangle^2). \quad (7)$$

Here $\alpha=a, b, c$ labels the three axis respectively. N is the number of the particles. m_α and P_α denote the average magnetization and polarization. χ_m^α and χ_e^α are the average magnetic and electric susceptibilities. C_m is the average specific heat. T represents the temperature and the Boltzmann constant k_B is absorbed into T .

We performed standard Monte Carlo simulation on an $L \times L'$ lattice with periodic boundary conditions. $L=100$ is the length of a zigzag chain and $L'=10$ is the number of the zigzag chains. It is assumed that a , b and c axes are respectively, along the directions of [100], [010], and [001]. The spin is updated according to the Metropolis algorithm. For every T , the initial 50000 Monte Carlo steps (MCS) are discarded for equilibration, and then the results are obtained by averaging 15000 data. Each data is collected at every 10 MCS.

The final results are obtained by averaging twenty independent data sets obtained by

selecting different seeds for random number generation.

III. RESULTS AND DISCUSSIONS

A. Ground state configuration and size effects

Similar to the measurement process in experiment [10, 11], the system is initially polarized by a small electric field $h_e=0.1$ along the c axis, which is implemented under the condition of the zero magnetic field cooling (ZFC). After that, the thermodynamic properties concerned in this paper are collected in a warming process with $h_e = 0.1$ along the c axis. The purpose of the poling procedure is to produce a single magnetoelectric domain with magnetic modulation vector along the chain. In fact, the spin-rotation axis of the spiral magnetic structure is with equal probability along $[110]$, $[\bar{1}\bar{1}0]$, $[1\bar{1}0]$, or $[\bar{1}10]$ direction. The choice depends on the sets of parameters. In the present simulation, due to a large negative magnetic anisotropy $D=-5$ in the diagonal of ab plane, the ground state composed of the spiral spin structure with spiral axis along the $[110]$ direction is generated.

Figure 3(a) presents the typical snapshot for the spin configuration at lowest temperature, demonstrating the formation of the spiral order at ground state. In order to analyze the spiral spin state accurately, the zero-field spin structure factor $S(q)$ is evaluated to scrutinize the microscopic magnetic structure and size effects. Since this compound possesses a weak J_{\perp} interaction and the spiral order is formed along the chain direction, $L' = 10$ is fixed in the present simulation for convenience. The lattice with different sizes $L=30-200$ is examined by $S(q)$ which is calculated along the chain direction with its expression written as[33]

$$S(q) = \sum_{i,r} \cos(q \cdot r) \langle \mathbf{S}_i \cdot \mathbf{S}_{i+r} \rangle, \quad (8)$$

where q is wave vector. r is calculated in units of distance between two nearest-neighbor correlated spins. In the inset of Fig. 3(b), $S(q)$ obtained in the lattice of $L = 100$ at $T = 0.01$ is plotted. The sharp characteristic peaks appear at $q_B = 0.3(\pi)$ and its equivalent position in $2\pi - q_B$, which confirm a good spiral spin order formed in ground states, as shown in Fig. 3(a). In addition, it is worth noted that the wavelength of spin structure will be limited by the periodic boundary condition, therefore the lattice size dependence of wave vector q_B is

examined to verify the perfect spiral spin structure. As shown in Fig. 3(b), the value of q_B vibrates with L varying, and the amplitude of vibration decreases as L increases. When L exceeds 80, the wave vector remains in the same position and the vibration disappears, indicating the negligible size effects under this circumstance. Thus, $L = 100$ chose here is adequate for the discussion of magnetoelectric properties in this system. To further confirm the conclusion above, the thermal dependence of the bulk properties for different lattice sizes under $h \parallel c$ are also displayed in Fig. 4. It can be seen that the results obtained with lattice size $L = 100$ are almost identical with those obtained from larger lattice size.

B. Compare to experimental results

In the following, we will concentrate on the magnetoelectric properties of LiCu_2O_2 from two aspects: the macroscopic thermodynamic behaviors and microscopic magnetic and ferroelectric structures. For the former, the simulation results on the bulk properties will be made a detail comparison with those of experimental results to reveal the spiral spin order nature of the ferroelectricity. As for the latter, our focus is on the influences of the exchange couplings and anisotropies on the spiral spin states, which will be explored by evaluating the spin structure factors.

In Fig. 5, the temperature dependence of magnetization m and susceptibility χ_m under a small magnetic field are presented. It can be seen that our simulation result is qualitatively in good agreement with experimental data in two aspects. First, m (χ_m) for $h \parallel c$ exceeds that for $h \parallel a, b$, reproducing the anisotropic behaviors observed in LiCu_2O_2 [8, 10]. Moreover, the negligible differences in the magnetization data between a and b axis are also in accord with recent report on untwinned crystals [13]. Second, at intermediate temperature, for all three field directions, a broad maximum presents in the m and χ_m curves, indicating the short-range antiferromagnetic correlations of the low-dimensional system. With the temperature increasing, a high-temperature Curie-Weiss susceptibility is exhibited. In addition, it is worth noted that the ratio of J_1/J_4 here is great than 1, suggestive of a strong "rung" coupling in this compound.

To make a full comparison, in Fig. 6 we present the results of the spontaneous polarization \mathbf{P} and its electric susceptibility χ_e along the c axis, as well as the specific heat C_m of the system. Similar to the experimental discovery, the two magnetic phase transitions

are also observed in our specific heat data. For convenience and uniformity, the lower-temperature phase is marked as T_{N2} and the other is marked as T_{N1} . As shown in Fig. 6(a), the main characteristics of P_c observed in LiCu_2O_2 are qualitatively reproduced based on the spin-current model. Below the transition temperature T_{N2} , P_c gradually emerges and is accompanied by the sharp peak arising in electric susceptibility χ_e^c (Fig. 6(b)) and specific heat (Fig. 6(c)), and then rises rapidly and almost reaches saturation below a lower temperature. When the system is polarized by an opposite electric field, P_c is reversed as well, indicating the ferroelectric nature of spiral order phase [19]. However, the reported remarkable field effects on the electric polarization [7] have not been exhibited in our results. As shown in Figs. 6(a) and (b), P_c and χ_e^c display the negligible responses for the field applied along different directions. This discrepancy implies the profound effects of the quantum fluctuations in LiCu_2O_2 . In the specific heat data, the phase transition at T_{N1} is exhibited and indicated by the smaller and round peak. Experimentally, it is found that this transition is associated with collinear spin structure with the spins sinusoidally modulated along the c axis. Its origin has not been explored yet. In the following, a conjecture and corresponding analysis on the possibilities that induce this transition will be given.

C. The effects of various exchange interactions and exchange anisotropy

In multiferroic system, spiral spin order is a common way to induce the ferroelectricity and always yields some surprising physical properties, such as flop, reversal and rotation of the electric polarization in an external magnetic field. It usually generated by the frustration in the magnetic materials, which origins from the competition of various interactions. Therefore, analyzing the impacts of different couplings on the spiral spin states is helpful to understand the magnetoelectric properties in multiferroics.

1. "Rung" coupling J_1

Figure 7(a) displays the influences of the "rung" coupling J_1 on the two transitions of the magnetic specific heat C_m . From a general view, the two transition temperatures suffer the slight affections and almost keep at the original positions, while their corresponding peak values present the different responses. The transition of T_{N1} shows the ignorable variations,

but the transition of T_{N2} exhibits the complex dependent relation on J_1 . For the sake of discussion, a parameter $\alpha=J_1/J_4$ is introduced here. One can see that for $\alpha \geq 1$, an evident suppression on the peak of T_{N2} is presented. The ability of the system resisting the thermal fluctuations is enhanced as well. While below $\alpha=1$, the transition at T_{N2} has no response to the variation of J_1 . These phenomenon are confirmed by the spin structure factors in Figs. 7(b) and (c). At $\alpha=1$, the peak of $S(q)$ moves towards large q with its intensity decreasing, indicating the modulated period of the incommensurate spin structure shortened by enhancing J_1 . These variations also demonstrate the fact that the spiral order can be significantly modified under the strong rung coupling. As α continues increasing, $S(q)$ shows very subtle decrease on its peak value, suggestive of a balance of the energy competition between the items of J_1 and J_4 . However, it is worth noted that a non-zero value appears at $q = 0$ for $\alpha \geq 1$, and it acts in a more obvious way with the increase of α , as shown inset of Fig. 7(c). This unusual dependence implies the arise of the low-temperature weak ferromagnetism.

2. Next-nearest-neighbor inchain interactions J_4

For a classical spin chain, when $|J_4/J_2|$ is larger than a critical value $1/4$, an incommensurate spiral spin structure with pitching angle $2\pi\xi = \arccos(1/|4J_4/J_2|)$ can be expected at ground state [7]. And therefore the changes of J_4 will evidently modify the magnitude of ξ and are macroscopically reflected in the variations of magnetic phase patterns. As shown in Fig. 8(a), the two magnetic phase transitions both shift towards high temperature with the increasement of J_4 . The peak at T_{N2} transition becomes sharp and is greatly strengthened, indicating the major adjustment of the spiral spin order, while the one at T_{N1} remains in a round shape and its almost constant height. This is also vividly demonstrated in the picture of the spin structure factors (Fig. 8(b)). When the value of J_4 is very close to that of J_1 , the peak of $S(q)$ is remarkably enhanced and moves towards large q . As J_4 further increases, the peak of $S(q)$ continues shifting to large value of q with its intensity invariant. This implies the reduction of the modulated period and the improvement of spirality between nearest-neighbor spins. In other words, it means the increasement of the pitch angle and macroscopically enhancement of the polarization, which is also well confirmed by our simulation results P_c (not shown here). In addition, at $q = 0$, $S(q)$ starts at a small value

and approaches to zero finally, reflecting the furious competition between J_4 and J_1 , which has been analyzed in Fig. 7.

3. exchange anisotropy Δ

Easy-plane anisotropy can enhance chiral correlation and is expected to exist in the edge-sharing spin-chain compounds. For example, in LiCuVO_4 , a prominent of easy-plane anisotropy is probed by ESR [26]. This anisotropy is expected to pin the spins to the ab plane, which is also verified in experiment. In our simulation, we find that it is also an indispensable factor for the occurrence of two phase transitions. In Fig. 9, the temperature dependence of C_m for different anisotropies Δ are presented. Here the "rung" coupling $J_1 = 2.4$ is made as the effects of the anisotropy are more obvious in this way and the results are qualitatively similar to those of $J_1 = 3.4$. As is shown, two humps appear with the anisotropy introduced. With the increase of Δ , one of the two humps becomes sharp and moves to a higher temperature while the other keeps almost at the original place. At $\Delta = 0.9$, the two subpeaks merge into one, implying the existence of the quasi-long-range spiral order and also indicated in the electric susceptibility (not shown here). In fact, even though the easy-plane anisotropy enhanced the spiral order, it suppresses the coupling between spin along the c axis, which is disadvantage for the formation of the polarization. However, because of the large magnitude of magnetic anisotropy D chosen in this simulation, it makes sure the strong spin coupling along the c axis, stabilizing the electric polarization arising at low temperature. Worth to mentioned, we find that the easy-plane anisotropy is a critical factor of inducing phase transition at T_{N1} , as it can generate the competition of energies from the ab plane spin coupling and the c axis spin coupling. Certainly, whether the spin configuration is sinusoidal modulation at this phase transition is still need further investigation. And we will discuss it in somewhere else.

To analyze the variations of the microscopic magnetic and ferroelectric structures, the q dependence of $S(q)$ for different Δ is calculated as shown in Fig. 10. At $\Delta=0.4$, the maximum and sharp peak at $q=0.32\pi$ indicates the domination of spiral order at T_{N2} . It worth noted that another two tiny peaks also appear at $q=0.02\pi$ and $q=\pi$ respectively, which suggestive of the existence of other possible magnetic phases at ground state. Since our focus is on the spiral order in this paper, the reason on the appearance of these two phases will

not be discussed here. With the increase of Δ , the magnetic phase at low temperature manifests as enhanced spiral order mixed with weak ferromagnetism. As $\Delta \geq 0.7$, only two characteristic sharp peaks appearing at q_B and its equivalent position $2\pi - q_B$ signify the formation of the quasi-long-ranged spiral order. To have a close view, the magnified of the collective behaviors of $S(q)$ for various Δ are presented in Fig. 11. As Δ increases, the tiny and round peak is enhanced and become sharp with a shift towards small value of q , indicating the increasement of the modulated period of spiral order. At $\Delta=0.7$ and $\Delta=0.8$, the peak height keeps constant and in the same position. A stable spiral order seems to be formed under this circumstance. However, when Δ continues increase, the peak of $S(q)$ with its invariant height shifts to large q , demonstrating the complexity of Δ on the magnetic ordered states.

IV. CONCLUSION

In summary, based on the ellipsoidal spiral structure at ground state, we qualitatively reproduce the complicated magnetoelectric behaviors observed in LiCu_2O_2 by performing Monte Carlo simulation. Our results indicate that the spin current model or the inverse Dzyaloshinskii-Mariya mechanism still works even though large quantum fluctuation exists in this compound. The spin structure factors have been evaluated to confirm the spiral spin order at lowest temperature and detect the variations of the microscopic magnetic structure. The divers effects of the different exchange couplings and exchange anisotropies on the magnetic patterns have been vividly demonstrated in this simulation. It turns out that the "rung" coupling J_1 can not be simply neglected, and the exchange anisotropy has a complicated influences on the magnetic order. Besides, the deviation of the field responses of the polarization from the experiment implies the importance of quantum fluctuation in this $S=1/2$ spiral magnet, which requires further studies on this interesting ferroelectric cuprate.

V. ACKNOWLEDGEMENTS

This work was supported by Academic Scholarship for Doctoral Candidates of China (Grant No. 10145201103), the Fundamental Research Funds for the Central Universities of China (Grant No. N110605002) and Shenyang Applied Basic Research Foundation (Grant No. F12-277-1-78) of China.

-
- [1] T. Kimura, T. Goto, H. Shintani, K. Ishizaka, T. Arima, Y. Tokura, *Nature (London)* **426**, 55 (2003).
 - [2] N. Hur, S. Park, P. A. Sharma, J. S. Ahn, S. Guha, S. W. Cheong, *Nature (London)* **429**, 392 (2004).
 - [3] R. Bursill, G. A. Gehring, D. J. J. Farnell, J. B. Parkinson, T. Xiang and C. Zeng, *J. Phys. Condens. Matter* **7**, 8605 (1995).
 - [4] M. Enderle, C. Mukherjee, B. Fäk, R. K. Kremer, J.-M. Broto, H. Rosner, S.-L. Drechsler, J. Richter, J. Malek, A. Prokofiev, W. Assmus, S. Pujol, J.-L. Raggazzoni, H. Rakoto, M. Rheinstädter, and H. M. Rønnow, *Europhys. Lett.* **70**, 237 (2005).
 - [5] S.-L. Drechsler, O. Volkova, A. N. Vasiliev, N. Tristan, J. Richter, M. Schmitt, H. Rosner, J. Málek, R. Klingeler, A. A. Zvyagin, and B. Büchner, *Phys. Rev. Lett.* **98**, 077202 (2007).
 - [6] M. G. Banks, F. Heidrich-Meisner, A. Honnecker, H. Rakoto, J.-M. Broto, and R. K. Kremer, *J. Phys. Condens. Matter* **19**, 145227 (2007).
 - [7] S. Park, Y. J. Choi, C. L. Zhang, and S-W. Cheong, *Phys. Rev. Lett.* **98**, 057601 (2007).
 - [8] A. A. Bush, V. N. Glazkov, M. Hagiwara, T. Kashiwagi, S. Kimura, K. Omura, L. A. Prozorova, L. E. Svistov, A. M. Vasiliev, and A. Zheludev, *Phys. Rev. B* **85**, 054421 (2012).
 - [9] S.-L. Drechsler, J. Málek, J. Richter, A. S. Moskvin, A. A. Gippius, and H. Rosner, *Phys. Rev. Lett.* **94**, 039705 (2005).
 - [10] Y. Yasui, K. Sato, Y. Kobayashi, and M. Sato, *J. Phys. Soc. Jpn.* **78**, 084720 (2009).
 - [11] Y. Kobayashi, K. Sato, Y. Yasui, T. Moyoshi, M. Sato, and K. Kakurai, *J. Phys. Soc. Jpn.* **78**, 084721 (2009).
 - [12] K.-Y. Choi, S. A. Zvyagin, G. Cao, and P. Lemmens, *Phys. Rev. B* **69**, 104421 (2004).
 - [13] H. C. Hsu, H. L. Liu, and F. C. Chou, *Phys. Rev. B* **78**, 212401 (2008).

- [14] L. Zhao, K.-W. Yeh, S. M. Rao, T.-W. Huang, P. Wu, W.-H. Chao, C.-T. Ke, C.-E. Wu, and M.-K. Wu, *E. P. L.* **97**, 37004 (2012).
- [15] T. Masuda, A. Zheludev, A. Bush, M. Markina, and A. Vasiliev, *Phys. Rev. Lett.*, **92**, 177201 (2004).
- [16] T. Masuda, A. Zheludev, B. Roessli, A. Bush, M. Markina, and A. Vasiliev, *Phys. Rev. B* **72**, 014405 (2005).
- [17] L. Mihály, B. Dóra, A. Ványolos, H. Berger, and L. Forró, *phys. Rev. Lett.* **97**, 067206 (2006).
- [18] A. Rusydi, I. Mahns, S. Müller, M. Rübhausen, S. Park, Y. J. Choi, C. L. Zhang, S.-W. Cheong, S. Smadici, P. Abbamonte, M. v. Zimmermann, and G. A. Sawatzky, *Appl. Phys. Lett.* **92**, 262506 (2008).
- [19] S. Seki, Y. Yamasaki, M. Soda, M. Matsuura, K. Hirota, and Y. Tokura, *Phys. Rev. Lett.* **100**, 127201 (2008).
- [20] D. V. Dmitriev and V. Ya. Krivnov, *Phys. Rev. B* **73**, 024402 (2006).
- [21] M. H. Qin, Y. J. Guo, S. Dong, K. F. Wang, and J.-M. Liu, *J. Appl. Phys.* **105**, 07D908 (2009).
- [22] J. Sirker, *Phys. Rev. B* **81**, 014419 (2010).
- [23] M. Chen and C. D. Hu, *Phys. Rev. B* **84**, 094433 (2011).
- [24] R. Maurice, A.-M. Pradipto, C. de Graaf, and R. Broer, *Phys. Rev. B* **86**, 024411 (2012).
- [25] X.-Y. Chen, Q. Jiang, and Y.-Z. Wu, *Solid State Commun.* **121**, 641 (2002).
- [26] H.-A. Krug von Nidda, L. E. Svistov, M. V. Eremin, R. M. Eremina, A. Loidl, V. Kataev, A. Validov, A. Prokofiev, and W. Aßmus, *Phys. Rev. B* **65**, 134445 (2002).
- [27] T. Masuda, A. Zheludev, A. Bush, M. Markina, and A. Vasiliev, *Phys. Rev. Lett.* **94**, 039706 (2005).
- [28] S. W. Huang, D. J. Huang, J. Okamoto, C. Y. Mou, W. B. Wu, K. W. Yeh, C. L. Chen, M. K. Wu, H. C. Hsu, F. C. Chou, and C. T. Chen, *Phys. Rev. Lett.* **101**, 077205 (2008).
- [29] M. Mostovoy, *Phys. Rev. Lett.* **96**, 067601 (2006).
- [30] H. Katsura, N. Nagaosa, and A. V. Balatsky, *Phys. Rev. Lett.* **95**, 057205 (2005).
- [31] C. Jia, S. Onoda, N. Nagaosa, and J. H. Han, *Phys. Rev. B* **76**, 144424 (2007).
- [32] H. J. Xiang and M.-H. Whangbo, *Phys. Rev. Lett.* **99**, 257203 (2007).
- [33] X. Yao, *EPL (Europhysics Letters)*, **94**, 67003 (2011).

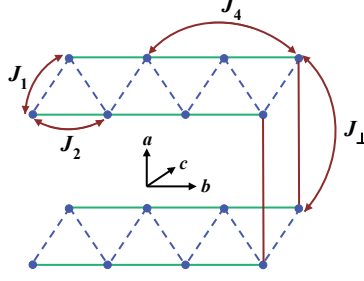


FIG. 1: (Color online) A schematic view of exchange interactions between magnetic Cu^{2+} ions in LiCu_2O_2 .

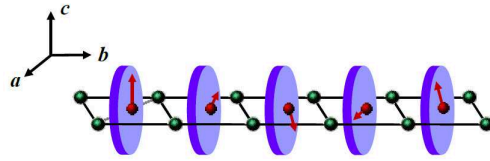


FIG. 2: (Color online) Schematic view of the spin configuration of LiCu_2O_2 in the ground state. The green and red balls represent O^{2-} and Cu^{2+} ions, respectively.

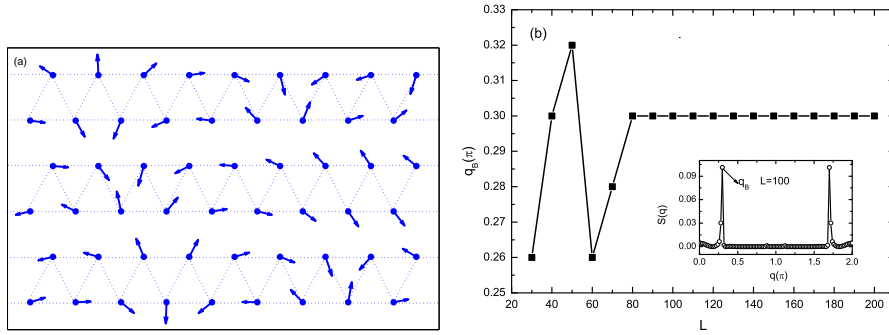


FIG. 3: (Color online) (a) A projection of the spin configuration to the bc plane at $T=0.01$. (b) The lattice size dependence of wave vector q_B at $T=0.01$. The inset is spin structure factor $S(q)$ for $L = 100$.

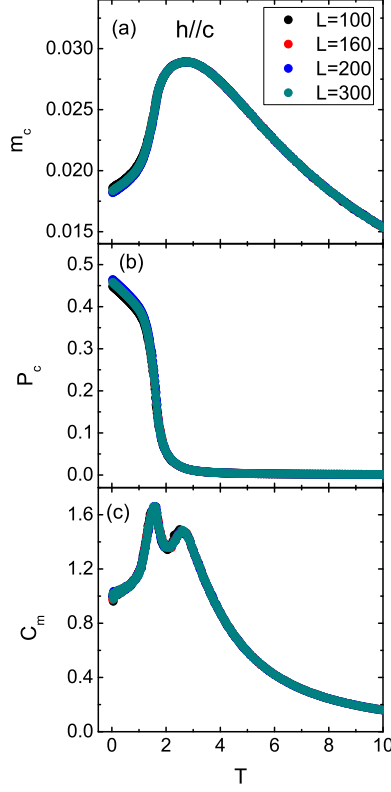


FIG. 4: (Color online) Temperature dependence of the magnetization, polarization and magnetic specific heat for different lattice sizes L with $h = 0.5$ applied along c axis.

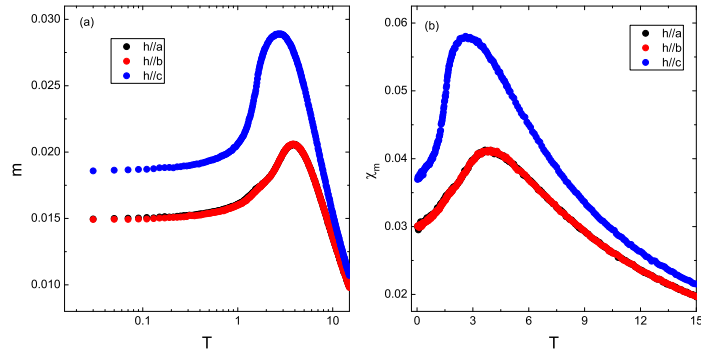


FIG. 5: (Color online) Temperature dependence of the magnetization curves (a) and susceptibility curves (b) under $h = 0.5$ and applied along three axis respectively.

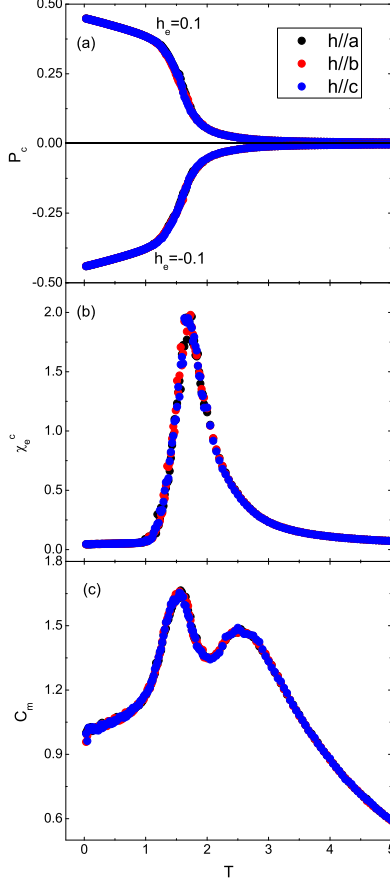


FIG. 6: (Color online) Temperature dependence of (a) the polarization P_c along the c axis, (b) the corresponding electric susceptibility χ_e^c and (c) the magnetic specific heat C_m for three field directions under $h=0.5$.

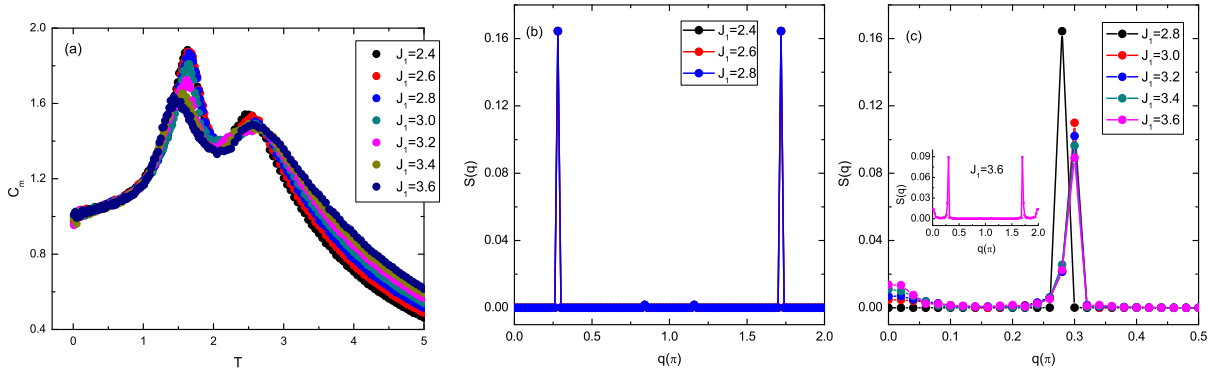


FIG. 7: (Color online) (a) Temperature dependence of the magnetic specific heat with the field $h = 0.5$ applied along the c axis for different "rung" coupling J_1 . (b), (c) Spin structure factors for different "rung" couplings at $T = 0.01$. The inset is the spin structure factor $S(q)$ for $J_1 = 3.6$.

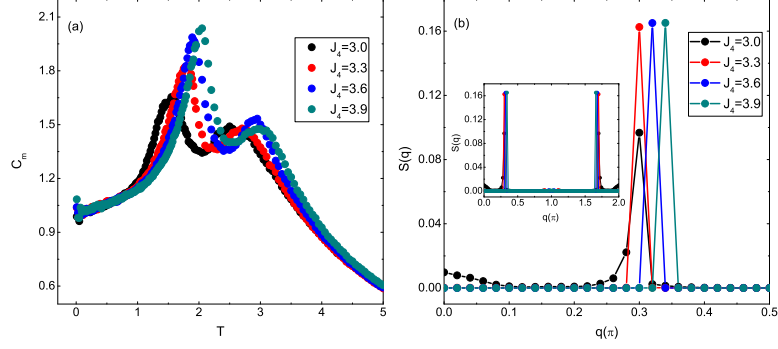


FIG. 8: (Color online) (a) Temperature dependence of the magnetic specific heat with the field $h = 0.5$ applied along the c axis and (b) spin structure factors $S(q)$ at $T = 0.01$ for different next-nearest neighbor inchain coupling J_4 . The inset is the full view of spin structure factors $S(q)$.

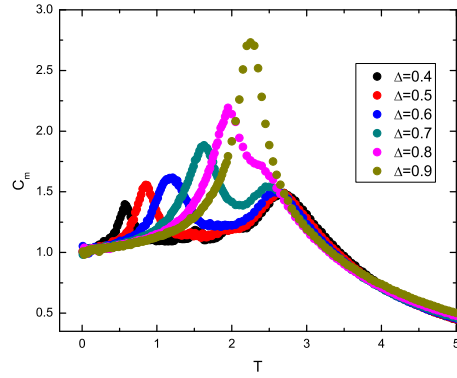


FIG. 9: (Color online) Temperature dependence of the magnetic specific heat with the field $h = 0.5$ applied along the c axis for different anisotropic coupling Δ .

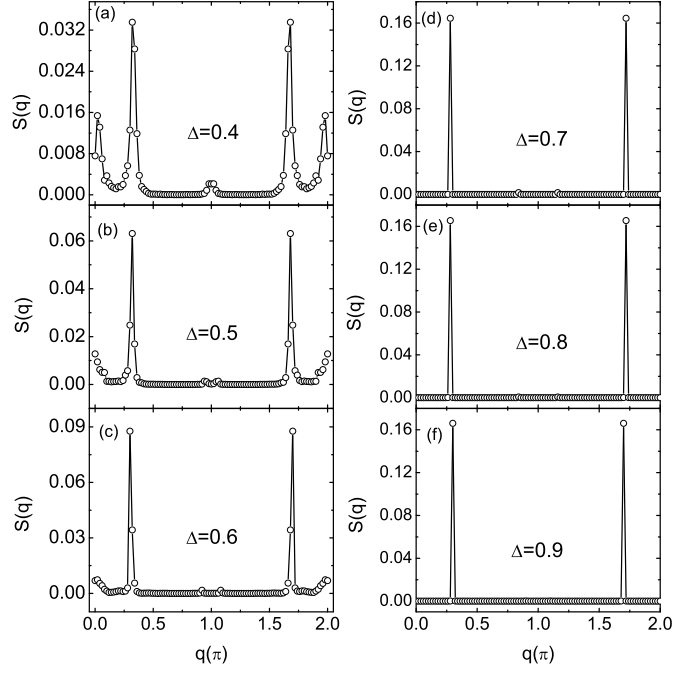


FIG. 10: (Color online) (a)-(f) The wave vector dependence of spin structure factor $S(q)$ for different exchange anisotropic couplings Δ at $T = 0.01$.

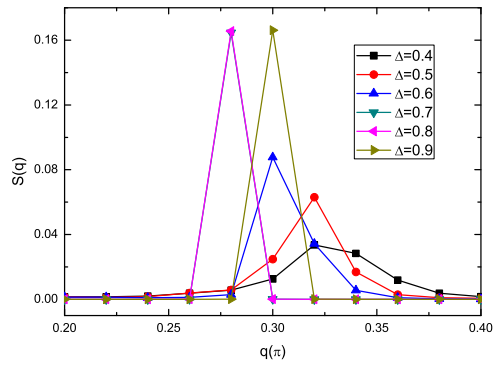


FIG. 11: (Color online) The enlarged view of spin structure factors $S(q)$ under various exchange anisotropies Δ .